METHODS **25,** 303–308 (2001)
doi:10.1006/meth.2001.1242, available online at http://www.idealibrary.com on IDEAL®

Construction of Low-Resolution X-Ray Crystallographic Electron Density Maps of the Ribosome

Jamie H. D. Cate[1]

Departments of Chemistry and Molecular and Cell Biology, University of California at Berkeley, Berkeley, California 94720

Advances in X-ray crystallography now allow biological macromolecules of almost any size to be imaged at atomic resolution. Here, I outline the strategy that allowed for the solution of the 70S ribosome structure to 7.8-Å resolution. The most important factors involve the effective use of synchrotron radiation and the application of existing crystallographic software to very large structures.

Many biological processes depend on the function of macromolecular complexes that are asymmetric and that can be quite large. Although cryo-electron microscopy (EM) images of these complexes are now reaching subnanometer resolution in many cases, crystallography presently provides the only means for obtaining atomic resolution images of biological macromolecules (1). Recently, structures of the ribosome (2) and ribosomal subunits have been determined by X-ray crystallography (3–7). Although the ribosomal subunits are now known at atomic resolution, much was learned about translation from the lower-resolution images generated along the way (2, 8–10) and from cryo-EM reconstructions (11, 12). In this review, the key steps in constructing images of complexes as large as the 70S ribosome by X-ray crystallography are reviewed.

Apart from obtaining well-diffracting crystals of biological molecules, the most difficult aspect of X-ray crystallography has been the determination of structure factor phases. Whereas structure factor amplitudes can be calculated directly from the observed diffraction intensities, the phases have to be derived from indirect experimental approaches (13). Strategies used to solve the structures of the ribosome or ribosomal subunits have involved variations of common tactics to determining phases and are applicable to structures of any size. The two most powerful approaches are multiwavelength anomalous dispersion (MAD) phasing and density modification algorithms. For very large complexes, these tools are still the best means to obtaining the highest quality electron density maps.

It should be noted that to solve the structures of the 30S and 50S ribosomal subunits and the 70S ribosome, computer programs written for smaller macromolecule X-ray crystallographic analysis were quite adequate for the larger structures (2, 3, 5). With few exceptions, only minor modifications, such as to array sizes, were needed. In this review, I highlight the software used to determine the structure of the 70S ribosome to 7.8 Å, much of which was also used in solving the structures of the ribosomal subunits. I also indicate those areas where further research may improve the capabilities of existing X-ray crystallography software to handle large structures.

THE IMPORTANCE OF MEASURING LOW-RESOLUTION DIFFRACTION INTENSITIES

To take advantage of MAD phasing and density modification, problems as large as the 70S ribosome may first require an initial solution of the phase problem at low resolution. In the cases of the 50S ribosomal subunit and 70S ribosome structures, images generated by electron microscopy provided initial structure factor phases to approximately 20-Å resolution (2, 9). The cryo-EM

[1] To whom correspondence should be addressed at Department of Chemistry, University of California, Berkeley, Lawrence Berkeley National Laboratory, Calvin Laboratory, 1 Cyclotron Road Mailstop, Berkeley, CA 94720. Fax: (510) 486-6240. E-mail: jcate@lbl.gov.

1046-2023/01 $35.00

images can be thought of as a starting molecular replacement model, or can at least define the molecular envelope of the structure within the crystal unit cell.

To make use of cryo-EM images, it is necessary to measure X-ray diffraction from crystals to very low resolution. Without the very low resolution structure factor terms included, severe Fourier transform ripples will occur in the electron density map, effectively wiping out any interpretable information (Fig. 1) (14–16). For example, since the dimensions of the 70S ribosomal particle exceed 200 Å in all directions, it was necessary to measure diffraction near 250-Å resolution (2). The structure factor intensities at this resolution can be extremely strong because they match the dimensions of the particle. Analysis of these very low resolution terms was useful in determining the packing of the ribosomes in the crystal unit cell (2). An important example of this kind of analysis has also been given for the structure of the nucleosome core particle (17).

Accurate measurement of low-resolution diffraction can be challenging when the unit cell is very large. For example, the X-ray optics and the position of the area detector are usually optimized for smaller macromolecule problems. At synchrotron beamlines with divergent X-ray sources (bending magnet or wiggler lines), it is necessary to collimate the X-ray beam near the X-ray mirrors and far upstream of the crystal position to limit the milliradians of X-rays impinging on the crystal (Fig. 2). Alternatively, or in addition, it is useful to focus the X-ray beam on the detector to minimize the diffraction spot shape relative to the area detector surface. For the structure of the 70S ribosome to 7.8 Å, we took advantage of the former approach at the Advanced Light Source beamline 5.0.2 (2).

For initial molecular replacement searches, it is not hard to measure diffraction at low resolution with sufficient accuracy, within the context of a single crystal, constant cryostabilizer, and use of a narrow range of X-ray wavelengths. We have found that the R_{sym} values for the very low diffraction measurements, for which there are still dozens of structure factor terms available for statistical analysis, are generally 2 to 4%. The experimental approach taken was simply to use a beam stop attached to a thin strip of mylar or kapton film. The beam stop was then placed close to the X-ray detector surface or as far from the crystal as necessary to allow low-angle X-ray diffraction to pass. At synchrotron beamlines, it is important to attenuate the X-ray beam almost completely, to avoid saturation of the detector by the strongest low-resolution diffraction. Nevertheless, measurement of the low-resolution diffraction at the synchrotron is critical, since it allows all the diffraction data to be measured from the same crystal at the same X-ray wavelength. As a result, the dynamic range necessary for a complete diffraction experiment may be more than seven to eight orders of magnitude.

EM IMAGES FOR MOLECULAR REPLACEMENT SEARCHES

The structures of the 70S ribosome and 50S ribosomal subunit, at early stages of the structure solution process, relied on molecular replacement with models based on cryo-EM images. In each case a slightly different strategy was used to convert the electron density generated from cryo-EM images into a model suitable for X-ray crystallography (2, 9). In the case of the 70S ribosome structure, the original cryo-EM image (18) was modeled as a collection of pseudo-atom X-ray scatterers. In practical terms, the electron density map was converted into a PDB file (see http://www.rcsb.org/pdb). In this way, subsequent steps of the crystallographic problem could be treated like any other molecular replacement problem. It is much harder to rotate and

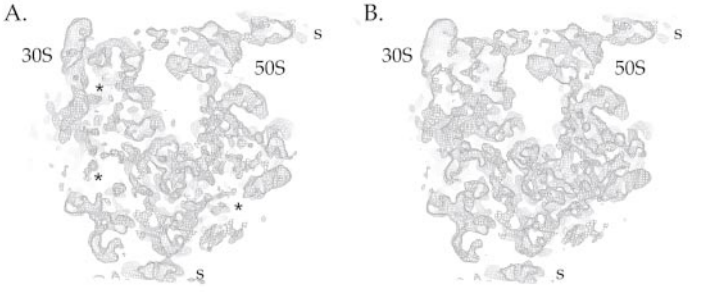

FIG. 1. Effect of very low resolution structure factors on the electron density map of the ribosome. (A) Section through the electron density map of the 70S ribosome using structure factors from 80- to 7.8-Å resolution. Asterisks mark regions of density that are suppressed in the absence of the low-resolution terms. Symmetry-related ribosomes in the crystal are marked "s" in the figures. (B) The same section through the electron density map of the 70S ribosome using structure factors from 300- to 7.8-Å resolution.

translate electron density maps than it is to move atomic (or pseudo-atomic) models through the unit cell. Atomic coordinates can be multiplied by a simple transformation matrix, whereas electron density maps require additional steps of interpolation on a predefined grid (19, 20).

Any electron density can be modeled as a superposition of Gaussian distributions depending on the resolution required. Each Gaussian distribution can be centered by a vector representing a point scatterer that can be stored as an atom in a PDB file. For example, atomic form factors for each atom type usually employ the superposition of four Gaussian distributions for atomic resolution modeling (21). At lower resolution, each amino acid in a protein can similarly be modeled as a superposition of a few Gaussian distributions. These "globbic" scatterers substitute for amino acids quite well at resolutions below 3.5 Å, but fail to capture the necessary asymmetry at atomic resolution (22). At even lower resolution, globbic scatterers do not represent discrete units in a macromolecule but simply occupy the observed electron density distributions in an economical way. Conceptually, the conversion of a low-resolution electron density map into point scatterers is no different than other treatments proposed for *ab initio* structure factor phasing, low-resolution treatment of protein structures, or holographic reconstruction methods (16, 22, 23).

In practical terms, I used the program CNS to conduct the molecular replacement search (24). The cryo-EM generated electron density of the 70S ribosome at 23-Å resolution (18) was placed in a very large triclinic unit cell (space group *P*1) and was modeled as a collection of about 700 point scatters, each represented by a single Gaussian distribution. Briefly, two coefficients for a Gaussian distribution defining a new atom type were added to the atomic form factor file (scatter.lib, Fig. 3) provided with CNS. As could be expected for so few scatterers representing a large particle, the "width" or "temperature factor" of the Gaussian distribution used was quite large. Then, the Fourier transform of the cryo-EM electron density map was calculated to generate a set of structure factors that could be used as the "observed" structure factors in conjugate-gradient minimization within CNS. However, as opposed to typical X-ray crystallographic refinement, the position of the 700 scatterers was refined against a vector residual, to retain the phase information contained within the structure factors of the EM image (24). After exhaustive refinement, the resulting pseudo-atom scatterers gave a nearly perfect representation of the cryo-EM image at 23-Å resolution, including any errors that it might contain. This model, stored in PDB format, could then be used with standard molecular replacement software (AMORE, CNS) (24, 25). Examples of low-resolution molecular replacement search strategies have been described elsewhere (16).

HEAVY-ATOM DERIVATIVES FOR SUPRAMOLECULAR COMPLEXES

Molecular replacement models for the 50S and 70S ribosomes played critical roles in the process of extending the resolution of the electron density maps generated from the measured X-ray diffraction data (2, 9). They simplified the search for heavy-atom derivatives, necessary to solve the phase problem at higher resolution, by eliminating the need to work solely in Patterson

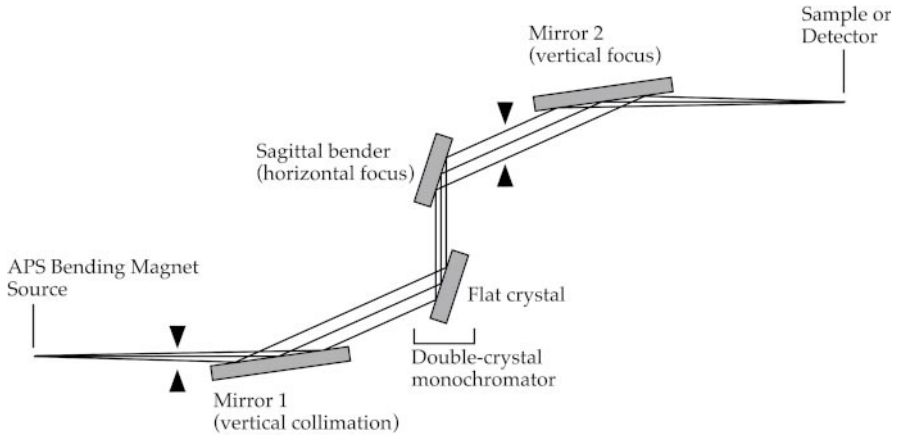

FIG. 2. Schematic diagram of beamline 8BM at the Advanced Photon Source. The beamline is designed to accept 1 milliradian of X-rays from the synchrotron source. Arrows mark the locations of slits that can be used to collimate the X-ray beam further. Control of a sagittal bender in the monochromator allows the X-rays to be focused on the crystal or the detector.

space. Electron-dense ("heavy") atoms bound to specific sites on a macromolecule can provide sufficient X-ray scattering to help determine structure factor phases in a diffraction experiment (26, 27). However, it is first necessary to locate the positions of heavy-atom compounds bound to a macromolecule within a crystal. Without prior structure-factor phase information, this search process must be carried out in Patterson space or by direct methods (28). Whereas direct method algorithms have worked to find heavy atom sites in complicated problems at 3-Å or better resolution (29, 30), it is unclear whether they can be optimized for searches at 7- to 15-Å resolution. Patterson space, which in a heavy atom search contains peaks representing vectors between all of the bound heavy atoms, becomes exponentially more crowded and difficult to deconvolute as the number of heavy atoms to be found increases (28). By moving the search for heavy atom binding sites to real electron density maps (Fourier difference maps (28)) which contain peaks at the positions of the heavy atoms, the molecular replacement models played a significant role in speeding the structure solution process. In the case of the 50S subunit structure, the EM-derived molecular replacement model helped confirm the positions of heavy atoms cluster compounds initially located in Patterson maps (9). In the 70S ribosome structure, the EM-derived molecular replacement model played a key role in identifying the first heavy-atom derivative in Fourier difference electron density maps, a tantalum cluster compound that bound to more than 20 sites on the 70S ribosome (2).

For lower-resolution electron density maps, and for very large structures, cluster compounds containing a large number of heavy atoms have been quite useful. Indeed, all of the X-ray crystal structures of ribosomal subunits or of the 70S ribosome relied on these cluster compounds for some structure-factor phasing information (2, 3, 5, 7). In the case of the 70S ribosome, only one cluster compound, $Ta_6Br_{12}^{2-}$ (31), proved useful, partly because other cluster compounds seriously degraded the diffraction quality of the crystals. At the resolution limit of approximately 11 Å, the tantalum cluster compound could be treated as a point scatterer, even for a MAD experiment (2). The anomalous signal from tantalum was used in this experiment, and structure-factor phases were determined in the program MLPHARE (32).

To obtain experimental structure-factor phase information to higher resolution, it is ultimately necessary to use more conventional heavy-atom compounds. In part, this is due to the fact that heavy-atom clusters cannot be modeled accurately at sufficiently high resolution if their binding is partially disordered (31). In practical terms, it may be the case that no cluster compound binds without degrading the crystal quality, as was observed for the 70S ribosome crystals (2). However, to obtain any phasing information from standard heavy-atom compounds, it may be necessary to bind dozens or even more than 100 heavy atoms to the supramolecular complex (2, 3, 5). At present, these sites can be found in Fourier difference electron density maps only by first determining structure-factor phases from cluster compounds and EM images at lower resolution, for example, to approximately 10 Å for the 70S ribosome structure (2). However, it may ultimately be possible to use direct method algorithms to locate this number of heavy atom sites in new structures, even at resolutions well below those typically used for direct method searches. Examples in which dozens of selenium or bromine sites have been identified by direct methods have been reported (29, 30).

In the case of the ribosome, composed of nearly two-thirds RNA, one class of compounds worked better than any other for three out of the four X-ray crystal structures. Three groups used osmium(III) hexammine or its chemical analog, iridium(III) hexammine, to obtain significant structure-factor phasing information (2, 3, 5). Osmium(III) hexammine, which preferentially binds in the major groove of RNA (33), was originally used in a MAD experiment to determine the structure of the group I intron P4–P6 domain (34). In the ribosomal subunit structures, this compound was used in a combination of multiple isomorphous replacement with anomalous dispersion (MIRAS) (3, 5). The 70S ribosome structure was determined to 7.8-Å resolution by performing a single MAD experiment with iridium(III)

```
SCATter ( chemical "X" )
  500.00  800.000 0.0000  0.00000  0.0000  0.0000 0.00000  0.0000  0.0000

SCATter ( chemical "O-1" )
  4.1916 12.8573 1.63969 4.17236 1.52673 47.0179 -20.307 -0.01404 21.9412
```

FIG. 3. Coefficients for a single Gaussian distribution in the file "scatter.lib" in CNS. The first coefficient corresponds to the number of electrons in the X-ray scatterer, while the second coefficient corresponds to the distribution of the electrons, or "width" of the Gaussian. Note that the temperature factor in a PDB file adds to the second term to increase the spread of the distribution of electrons. The trailing seven zeros correspond to three additional Gaussian distributions and a constant term usually used for atomic form factors, as shown for negatively charged oxygen in the second entry.

hexammine as the derivative (2). At nearly 2.5 MDa in size the ribosome provided a difficult test case for MAD phasing. Yet, once the majority of the heavy-atom sites had been located in Fourier difference electron density maps, standard heavy-atom refinement in MLPHARE (32) and residual electron density maps calculated using programs in CCP4 (20) were sufficient to calculate structure-factor phases to 7.8-Å resolution.

DENSITY MODIFICATION ALGORITHMS TO IMPROVE ELECTRON DENSITY MAPS

Although structure-factor phases derived from heavy-atom derivatives are essential for solving any macromolecular complex at lower than atomic resolution, the resulting structure factors will generally yield a marginal electron density map. It should be possible to distinguish the solvent areas from the macromolecule, for example, but that may be the limit of information that can be gleaned without density modification algorithms (Fig. 4). Density modification takes advantage of the fact that the solvent region between macromolecules in a crystal should be essentially flat due to solvent disorder, and should have a lower mean electron density relative to the macromolecule (13). Typically, the initial electron density is adjusted mainly in the solvent region to remove noise peaks. The Fourier transform of the resulting electron density map generates structure factors whose phases are recombined with the original phases. This process is then repeated with the new phase set for a defined number of cycles, finally yielding dramatically improved structure factors and a high-quality electron density map. For the 70S ribosome structure determination, new algorithms that proved effective in solving the structure of the F1-ATPase complex significantly improved the final electron density map of the ribosome at 7.8-Å resolution (13, 24, 35). These algorithms have recently allowed us to extend the resolution of the structure to approximately 5.5-Å resolution (36).

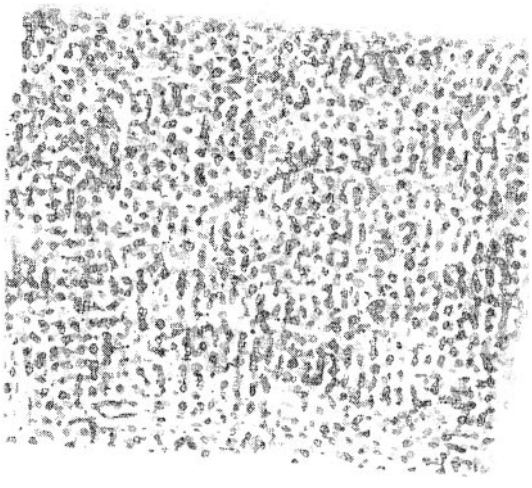

FIG. 4. Electron density map of the 70S ribosome prior to density modification. Structure factors from 80- to 7.8-Å resolution and with phases determined in the program MLPHARE were used to calculate the map. The section of the map and orientation, as well as the contouring level, are identical to those of Fig. 1. Note that heavy-atom phasing provided no useful phase information from 300- to 80-Å resolution.

The first step in applying density modification involves defining the boundary between the macromolecule and solvent. Although automated algorithms have been developed to define this envelope, or "mask," based on histograms of the initial electron density (35, 37), the initial EM image may provide a much more useful reference. For example, it is possible to use the starting pseudo-atom model to generate a mask in the program MAMA by choosing a suitably large atomic radius and applying smoothing functions available in the program (38). This mask can then be iteratively improved as the initial electron density is subjected to rounds of density modification. Without an atomic model to assist the process, it may be necessary to manually adjust the mask based on careful inspection of the initial electron density and subsequent maps. For example, tRNA ligands present in the X-ray structure of the 70S ribosome were initially not defined as part of the macromolecular region by the starting mask generated from the cryo-EM data (2, 18).

For the 70S structure determination, we used the program CNS to apply density modification to the structure factors (24). As was the case for the F1-ATPase structure, a "solvent flipping" algorithm with a gamma correction function (39) and sigmaA-weighted phase combination (40) worked extremely well. At low resolution, default parameters such as the ratio of mean electron density within the solvent to that in the macromolecule do not necessarily apply, however. Other parameters that can be changed include the percentage of density within the macromolecular region to truncate, to remove spurious low or high density in this region. One useful diagnostic is to adjust the mean solvent density of the electron density map to match the expected ratio of solvent and macromolecular density levels immediately prior to the Fourier transformation that precedes phase combination. I found that the best electron density maps were generated when the values for the truncation and solvent-to-macromolecule density ratio parameters (described in the CNS documentation) resulted in nearly zero adjustment of the mean solvent density level prior to each round of phase combination.

CONCLUSIONS

Supramolecular complexes make up a significant fraction of the functional units in biology, and are increasingly becoming the targets of X-ray crystallographic structure analyses. Once crystals of these complexes are obtained, it is now possible to combine cryo-EM reconstructions with X-ray diffraction measurements to generate starting structures at low resolution. With a few strategic adjustments to standard structure determination methods at synchrotron beamlines and in computational algorithms, it is now possible to extend the resolution of these structures from that of cryo-EM images to atomic resolution.

REFERENCES

1. Tao, Y., and Zhang, W. (2000) *Curr. Opin. Struct. Biol.* **10,** 616–622.
2. Cate, J. H., Yusupov, M. M., Yusupova, G. Z., Earnest, T. N., and Noller, H. N. (1999) *Science* **285,** 2095–2104.
3. Wimberly, B. T., Brodersen, D. E., Clemons, W. M., Jr., Morgan-Warren, R. J., Carter, A. P., Vonrhein, C., Hartsch, T., and Ramakrishnan, V. (2000) *Nature* **407,** 327–339.
4. Carter, A. P., Clemons, W. M., Jr., Brodersen, D. E., Morgan-Warren, R. J., Wimberly, B. T., and Ramakrishnan, V. (2000) *Nature* **407,** 340–348.
5. Ban, N., Nissen, P., Hansen, J., Moore, P. B., and Steitz, T. A. (2000) *Science* **289,** 905–920.
6. Nissen, P., Hansen, J., Ban, N., Moore, P. B., and Steitz, T. A. (2000) *Science* **289,** 920–930.
7. Schluenzen, F., Tocilj, A., Zarivach, R., Harms, J., Gluehmann, M., Janell, D., Bashan, A., Bartels, H., Agmon, I., Franceschi, F., and Yonath, A. (2000) *Cell* **102,** 615–623.
8. Clemons, W. M., Jr., May, J. L., Wimberly, B. T., McCutcheon, J. P., Capel, M. S., and Ramakrishnan, V. (1999) *Nature* **400,** 833–840.
9. Ban, N., Freeborn, B., Nissen, P., Penczek, P., Grassucci, R. A., Sweet, R., Frank, J., Moore, P. B., and Steitz, T. A. (1998) *Cell* **93,** 1105–1115.
10. Ban, N., Nissen, P., Hansen, J., Capel, M., Moore, P. B., and Steitz, T. A. (1999) *Nature* **400,** 841–847.
11. Frank, J. (2000) *Chem. Biol.* **7,** R133–R141.
12. van Heel, M. (2000) *Curr. Opin. Struct. Biol.* **10,** 259–264.
13. Abrahams, J. P., and De Graaff, R. A. (1998) *Curr. Opin. Struct. Biol.* **8,** 601–605.
14. Schevitz, R. W., Podjarny, A. D., Krishnamachari, N., Hughes, J. J., Sigler, P. B., and Sussman, J. L. (1979) *Nature* **278,** 188–190.
15. Podjarny, A. D., Schevitz, R. W., and Sigler, P. B. (1981) *Acta Crystallogr. Sect. A* **37,** 662–668.
16. Podjarny, A. D., and Urzhumtsev, A. G. (1997) *Methods Enzymol.* **276,** 641–658.
17. Finch, J. T., Lutter, L. C., Rhodes, D., Brown, R. S., Rushton, B., Levitt, M., and Klug, A. (1977) *Nature* **269,** 29–36.
18. Frank, J., Zhu, J., Penczek, P., Li, Y., Srivastava, S., Verschoor, A., Radermacher, M., Grassucci, R., Lata, R. K., and Agrawal, R. K. (1995) *Nature* **376,** 441–444.
19. Stein, P. E., Boodhoo, A., Armstrong, G. D., Cockle, S. A., Klein, M. H., and Read, R. J. (1994) *Structure* **2,** 45–57.
20. Collaborative Computational Project Number 4 (1994) *Acta Crystallogr. Sect. D* **50,** 760–763.
21. Maslen, E. N., Fox, A. G., O'Keefe, M. A., Brown, P. J., and Willis, B. T. M. (1999) *in* International Tables for Crystallography: Mathematical, Physical and Chemical Tables (Prince, E., and Wilson, A. J. C., Eds.), Vol. C, p. 992, Kluwer Academic, Dordrecht.
22. Guo, D. Y., Blessing, R. H., Langs, D. A., and Smith, G. D. (1999) *Acta Crystallogr. Sect. D* **55,** 230–237.
23. Somoza, J. R., Szöke, H., Goodman, D. M., Beran, P., Truckses, D., Kim, S. H., and Szöke, A. (1995) *Acta Crystallogr. Sect. A* **51,** 691–708.
24. Brünger, A. T., *et al.* (1998) *Acta Crystallogr. Sect. D* **54,** 905–921.
25. Navaza, J., and Saludjian, P. (1997) *Methods Enzymol.* **276,** 581–593.
26. Ke, H. (1997) *Methods Enzymol.* **276,** 448–461.
27. Hendrickson, W. A., and Ogata, C. N. (1997) *Methods Enzymol.* **276,** 494–523.
28. Drenth, J. (1999) Principles of Protein X-ray Crystallography, Springer Verlag, Heidelberg.
29. Uson, I., and Sheldrick, G. M. (1999) *Curr. Opin. Struct. Biol.* **9,** 643–648.
30. Dauter, Z., and Dauter, M. (2001) *Structure* **9,** R21–R26.
31. Schneider, G., and Lindqvist, Y. (1994) *Acta Crystallogr. Sect. D* **50,** 186–191.
32. Otwinowski, Z. (1991) *in* Isomorphous Replacement and Anomalous Scattering (Wolf, W., Evans, P. R., and Leslie, A. G. W., Eds.), pp. 80–86, Daresbury Laboratory, Warrington.
33. Cate, J. H., and Doudna, J. A. (1996) *Structure* **4,** 1221–1229.
34. Cate, J. H., Gooding, A. R., Podell, E., Zhou, K., Golden, B. L., Kundrot, C. E., Cech, T. R., and Doudna, J. A. (1996) *Science* **273,** 1678–1685.
35. Abrahams, J. P., and Leslie, A. G. W. (1996) *Acta Crystallogr. Sect. D* **52,** 30–42.
36. Yusupov, M. M., Yusupova, G. Z., Baucom, A., Lieberman, K., Earnest, T. N., Cate, J. H., and Noller, H. F. (2001) *Science* **292,** 883–896.
37. Wang, B. C. (1985) *Methods Enzymol.* **115,** 90–112.
38. Kleywegt, G. J., and Jones, T. A. (1999) *Acta Crystallogr. Sect. D* **55,** 941–944.
39. Abrahams, J. P. (1997) *Acta Crystallogr. Sect. D* **53,** 371–376.
40. Read, R. J. (1997) *Methods Enzymol.* **277,** 110–128.